Thermochemical and Kinetic Analysis of the Thermal Decomposition of Monomethylhydrazine: An Elementary Reaction Mechanism†

Hongyan Sun* and Chung K. Law

Department of Mechanical and Aerospace Engineering, Princeton University, Princeton, New Jersey 08544

Received: November 15, 2006; In Final Form: December 28, 2006

The reaction kinetics for the thermal decomposition of monomethylhydrazine (MMH) was studied with quantum Rice−Ramsperger−Kassel (QRRK) theory and a master equation analysis for pressure falloff. Thermochemical properties were determined by ab initio and density functional calculations. The entropies, $S°$(298.15 K), and heat capacities, $C_p°(T)$ ($0 \leq T/\mathrm{K} \leq 1500$), from vibrational, translational, and external rotational contributions were calculated using statistical mechanics based on the vibrational frequencies and structures obtained from the density functional study. Potential barriers for internal rotations were calculated at the B3LYP/6-311G(d,p) level, and hindered rotational contributions to $S°$(298.15 K) and $C_p°(T)$ were calculated by solving the Schrödinger equation with free rotor wave functions, and the partition coefficients were treated by direct integration over energy levels of the internal rotation potentials. Enthalpies of formation, $\Delta_f H°$(298.15 K), for the parent MMH (CH_3NHNH_2) and its corresponding radicals $CH_3N^{\bullet}NH_2$, $CH_3NHN^{\bullet}H$, and $C^{\bullet}H_2NHNH_2$ were determined to be 21.6, 48.5, 51.1, and 62.8 kcal mol^{-1} by use of isodesmic reaction analysis and various ab initio methods. The kinetic analysis of the thermal decomposition, abstraction, and substitution reactions of MMH was performed at the CBS-QB3 level, with those of N−N and C−N bond scissions determined by high level CCSD(T)/6-311++G(3df,2p)//MPWB1K/6-31+G(d,p) calculations. Rate constants of thermally activated MMH to dissociation products were calculated as functions of pressure and temperature. An elementary reaction mechanism based on the calculated rate constants, thermochemical properties, and literature data was developed to model the experimental data on the overall MMH thermal decomposition rate. The reactions of N−N and C−N bond scission were found to be the major reaction paths for the modeling of MMH homogeneous decomposition at atmospheric conditions.

1. Introduction

Hydrazine and its methyl derivatives are of interest because of their high-energy content, versatility, and reactivity. Specifically, being storable liquids, they are attractive as bipropellant fuels as well as monopropellants for thrusters used in long-term satellite and space activities. For example, monomethylhydrazine (MMH) is often used in association with nitrogen tetroxide for satellite propulsion.[1] Furthermore, as monopropellants, they decompose exothermically as soon as they come into contact with a catalyst or a hot surface, and generate hot gas in a controlled manner for thrust or pneumatic power.[2] Thus knowledge of the decomposition of hydrazines is not only valuable in predicting the storability and possible precombustion reactions, but it is also an essential component of the full kinetic mechanism needed for the modeling of propellant combustion applications.

Of the many modes of hydrazine decomposition, thermal and heterogeneous catalytic decompositions are the most practically important.[2] Several experimental studies on the thermal decomposition of hydrazine derivatives have been conducted. Specifically, in the 1960s Kerr et al.[3] studied the pyrolysis of hydrazine, MMH, and benzylamines at pressures of 0.01−0.04 atm by the toluene-carrier technique. Eberstein et al.[4] subsequently studied the gas-phase decomposition of hydrazine, monomethylhydrazine, and unsymmetrical dimethylhydrazine (UDMH) in an adiabatic flow reactor at atmospheric pressure and temperatures between 750 and 1000 K, and found that their decomposition rates are in the order UDMH > MMH > N_2H_4, while their overall reaction orders are very close to unity. In 1972, Golden et al.[5] experimentally studied the first-order disappearance of hydrazine methyl derivatives by the very low pressure pyrolysis (VLPP) technique (pressure 0.1−10 mTorr), and reported that MMH decomposes via molecular concerted elimination of NH_3 and H_2 rather than N−N bond scission. Recently, Catoire et al.[6−10] studied the ignition and detonation of mixtures of gaseous hydrazines and oxygen in shock tubes at temperatures of 850−1440 K and pressures of 160−400 kPa, and reported kinetic modeling results on their combustion experiments.

The decomposition of hydrazine derivatives is characteristic of the chemical bond energy released or suppressed from the N−N bond of the molecule. Little is known of the bond dissociation energies in the hydrazine system of compounds, and many elementary reactions that occur during propellant combustion are not well characterized. Accurate thermochemical property data and reaction kinetics of MMH decomposition are important for understanding their stability, reaction pathways, and fundamental reaction mechanisms. These considerations led to the objectives and focuses for the present study, namely to (1) determine accurate thermochemical properties and bond energies of MMH decomposition by using ab initio and density functional methods, (2) determine the rate parameters for primary dissociation and abstraction reactions on the MMH thermal decomposition, and (3) develop an elementary reaction

† Part of the special issue "James A. Miller Festschrift".

* Author for correspondence. Fax: (609) 258-6233. E-mail: hsun@princeton.edu.

10.1021/jp067591l CCC: $37.00
Published on Web 02/27/2007

mechanism of the thermal decomposition of MMH for further modeling of propellant combustion applications.

2. Calculation Methods

All of the density functional and ab initio calculations were carried out with the Gaussian 03 software package.[11] Several density functional and ab initio methods such as B3LYP/6-311G(d,p),[12] CBS-Q,[13] CBS-QB3,[14] G3,[15] G3B3,[16] G3MP2,[17] MPWB1K/6-31+G(d,p),[18] and CCSD(T)/6-311++G(3df,2p)[19] were used in isodesmic reaction analysis to determine the enthalpy of formation of the critical species in the thermal decomposition of MMH. The CBS-QB3 method was found to predict reliable enthalpy values of hydrazine compounds with less computational cost. The most stationary points of the potential energy surface and transition states of abstraction and substitution on the MMH decomposition were further calculated by using the CBS-QB3 method, and the bond energies of N−N and C−N bond scissions were calculated at the CCSD(T)/6-311++G(3df,2p) level with geometries optimized by the MPWB1K/6-31+G(d,p) method. The MPWB1K is a hybrid meta density functional theory developed by Truhlar et al.,[18] who demonstrated that it is a good method for themochemical kinetics. The complete basis set model CBS-QB3 of Petersson et al.[14] is a modified standard CBS-Q method, which uses B3LYP hybrid density functional structures and frequencies to achieve both enhanced reliability and improved accuracy. The standard CBS-QB3 method starts with B3LYP/6-311G(d,p) geometry optimization and frequency calculation, which is then followed by the single-point calculation at the CCSD(T)/6-31+G(d′), MP4(SDQ)/6-31+G(d(f),p), and UMP2/6-311+G-(3d2f,2df,2p) levels. This energy is then extrapolated to the complete basis set limit.

The total partition function of the target species was calculated with the framework of the rigid-rotor-harmonic-oscillator approximation with correction for internal rotation. The entropies and heat capacities from vibrational, translational, external rotational, and electronic contributions were calculated using statistical mechanics based on the vibrational frequencies and moments of inertia from the DFT optimized structures. All the torsional motions on the single bonds between the heavy atoms were treated as hindered internal rotations. The torsion frequencies were identified by viewing the bond motions using the GaussView program.[20] They were omitted in the calculation of $S°(298.15\ \mathrm{K})$ and $C_p°(T)$, but their contributions were replaced with values from analysis of the internal rotation potentials. The hindrance internal rotation potentials were obtained by varying the torsion angle in 15° intervals and allowing the remaining molecular structure parameters to be optimized at the B3LYP/6-311G(d,p) level. Subsequently, contributions from hindered rotors to $S°(298.15\ \mathrm{K})$ and $C_p°(T)$ were determined by solving the Schrödinger equation with free rotor wave functions, with the partition coefficients treated by direct integration over energy levels of the intramolecular rotational potential curves that are represented by a truncated Fourier series as $a_0 + \sum a_i \cos(i\varphi) + \sum b_i \sin(i\varphi)$ with $\varphi \leq 8$.

The values of the enthalpy of formation $\Delta H_f°_{298}$ for reactants and intermediate radicals were determined by using the total electronic energies from ab initio and DFT calculations and isodesmic reactions with group balance when possible. Isodesmic reactions are hypothetical reactions in which the number of electron pairs and bonds of the same type are conserved on both sides of the equation so that only the relationship among the bonds is altered. If the additive groups in each compound are also conserved on both sides of the equation, isodesmic reactions provide higher accuracy even at lower calculation levels because the nature of the bonds is conserved while the inherent errors associated with the computation of both reactants and products are as such partially canceled. The scaling factors of 0.9806, 0.9661, and 0.9537 were used to correct zero point vibrational energies (ZPVEs) determined from B3LYP/6-311G-(d,p), MP2(full)/6-31G(d,p), and MPWB1K/6-31+G(d,p) frequencies,[18,21] respectively. Transition state (TS) geometries were identified by the existence of only one imaginary frequency in the normal mode coordinate analysis, evaluation of the TS geometry, and the vibration motion of the reaction coordinates. The $\Delta_f H°(298.15\ \mathrm{K})$ values of the transition state structures were calculated by the $\Delta_f H°(298.15\ \mathrm{K})$ of the stable reactant from isodesmic reaction analysis, plus the difference of total energies between the reactant and transition states.

The enthalpies and entropies were treated with conventional transition state theory to calculate the Arrhenius preexponential factors and activation energies that result in high pressure limit rate constants (k_∞) as functions of temperature. The equilibrium constants $K_{eq}(T)$ were calculated from the thermodynamic properties of reactants and products as a function of temperature. The reverse rate constants were calculated from the principle of microscopic reversibility. The branching ratios of the thermally energized reactant to stabilization and product channels were calculated using multifrequency quantum Rice−Rampsperger−Kassel (QRRK) analysis for $k(E)$,[22,23] with the steady-state assumption of the energized adduct(s) in combination with a master equation analysis for pressure falloff.

To account for the quantum mechanical tunneling effect on the reaction rates at low temperatures, the tunneling factors were calculated by using Wigner's perturbation equation:[24]

$$\Gamma = 1 + \frac{1}{24}\left(\frac{h\nu}{k_B T}\right)^2\left(1 + \frac{k_B T}{E_c}\right)$$

where Γ is the tunneling factor, h is Planck's constant, k_B is the Boltzmann constant, ν is the imaginary asymmetric stretching frequency of the transition state, and E_c is the activation energy without zero point energy corrections. The tunneling factors were further used to correct the high pressure limit rate constants (k_∞), which were then fitted by three parameters, A, n, and E_a, over a temperature range of 300−2000 K, as expressed by $k_\infty = AT^n \exp(-E_a/RT)$.

3. Results and Discussion

3.1. Thermochemical Properties. The optimized geometric parameters for 28 species in the MMH reaction system at the B3LYP/6-311G(d,p) level are listed in Table S1 in the Supporting Information. The corresponding unscaled vibrational frequencies and moments of inertia are listed in Table 1. Several transition state structures failed to be located at the DFT level, but were found at the MP2(full)/6-31G(d,p) level of calculation, as shown in italics.

A. Enthalpies of Formation and Bond Energies. The enthalpies of formation of the parent MMH molecule and its corresponding radicals were calculated by isodesmic reaction analysis and various ab initio methods as shown in Table 2. The $\Delta_f H°(298.15\ \mathrm{K})$ of the MMH was calculated from the isodesmic reaction $CH_3NHNH_2 + NH_3 \rightarrow CH_3NH_2 + NH_2$-$NH_2$ at the B3LYP/6-311G(d,p), CBS-Q, CBS-QB3, G3, G3MP2, G3B3, MPWB1K/6-31+G(d,p), and CCSD(T)/6-311++G(3df,2p)//MPWB1K/6-31+G(d,p) levels. Table 2 shows that the calculated values are in good agreement at these different levels, with an average value of 21.6 ± 0.5 kcal mol^{-1}.

TABLE 1: Harmonic Vibrational Frequencies and Moments of Inertia for Species in the MMH Decomposition System

species	frequencies[a] (cm^{-1})	moments of inertia (amu $bohr^2$)
CH_3NHNH_2	265, 360,422,787, 927, 991, 1135, 1138, 1229, 1321, 1449, 1480, 1494, 1523, 1690, 2915, 3042, 3085, 3377, 3518, 3534	48.5, 187.5, 211.9
$CH_3N^{\bullet}NH_2$	163, 444, 477, 674, 957, 1057, 1102, 1283, 1318, 1426, 1478, 1480, 1653 , 2922, 2977, 3110, 3393, 3605	38.8, 172.3, 198.3
$C^{\bullet}H_2NHNH_2$	285, 365, 439, 661, 709, 898, 1015, 1234, 1256, 1328, 1460, 1506, 1685, 3119, 3232, 3417, 3525, 3567	39.0, 176.7, 202.6
$CH_3NHN^{\bullet}H$	207, 378, 487, 737, 958, 1123, 1146, 1275, 1414, 1452, 1478, 1510, 1551, 2977, 3058, 3102, 3385, 3569	38.9, 179.0, 204.5
$CH_2{=}NNH_2$	435, 517, 656, 788, 931, 1074, 1182, 1315, 1479, 1659, 1694, 3019, 3193, 3434, 3625	39.0, 176.7, 202.6
$CH_3N{=}NH$	198, 558, 865, 927, 1143, 1174, 1405, 1468, 1470, 1500, 1660, 3013, 3094, 3104, 3265	30.0, 162.5, 181.3
TS1	1357i, 229, 296, 359, 527, 814, 906, 992, 1122, 1187, 1422, 1446, 1455, 1511, 1541, 2677, 2861, 2884, 3052, 3517, 3652	52.1, 200.9, 232.9
TS2	1306i, 64, 235, 386, 523, 628, 731, 769, 1083, 1169, 1291, 1397, 1421, 1476, 1693, 2482, 3036, 3153, 3208, 3429, 3533	51.9, 270.0, 296.9
TS3	1203i, 217, 391, 515, 774, 793, 903, 1012, 1057, 1139, 1239, 1391, 1494, 1530, 1549, 2094, 3036, 3116, 3276, 3440, 3448	54.2, 182.2, 209.5
TS4	*199i, 385, 467, 561, 642, 743, 1061, 1088, 1146, 1172, 1253, 1313, 1432, 1525, 1642, 1713, 2078., 3083, 3211, 3579, 3725*	*49.6, 175.0, 207.4*
TS5	*1218i, 170, 396, 509, 623, 729, 962, 1012, 1095, 1144, 1207, 1282, 1449, 1475, 1511, 1565, 2602, 3047, 3147, 3237, 3342*	*50.3, 182.2, 217.1*
TS6	2124i, 108, 316, 376, 468, 707, 809, 932, 963, 1126, 1214, 1330, 1416, 1446, 1507, 2198, 3015, 3164, 3223, 3375, 3444	51.2, 257.8, 284.7
TS7	1252i, 40, 132, 172, 259, 307, 423, 489, 518, 573, 774, 960, 1064, 1121, 1142, 1217, 1305, 1334, 1421, 1425, 1440, 1479, 1498, 1559, 1668, 2936, 3035, 3060, 3098, 3201, 3208, 3450, 3559	208.8, 413.6, 561.5
TS8	377i, 113, 134, 170, 249, 306, 429, 551, 604, 759, 917, 1039, 1125, 1142, 1225, 1325, 1444, 1478, 1500, 1541, 1606, 1675, 1888, 2931, 3031, 3100, 3374, 3448, 3462, 3543	206.6, 395.9, 547.1
TS9	1114i, 71, 139, 172, 182, 253, 431, 607, 661, 844, 983, 1111, 1126, 1200, 1338, 1361, 1441, 1478, 1500, 1515, 1664, 2951, 3034, 3115, 3294, 3476, 3573	200.1, 369.7, 514.5
TS10	*2062i, 178, 452, 557, 862, 1009, 1089, 1106, 1190, 1355, 1429, 1475, 1487, 2486, 2972, 3026, 3106, 3295*	*41.4, 177.6, 202.1*
TS11	1411i, 31, 89, 150, 320, 367, 408, 466, 561, 651, 762, 918, 1020, 1102, 1151, 1188, 1245, 1320, 1412, 1418, 1444, 1452, 1466., 1508, 1687, 3036, 3052, 3112, 3184, 3186, 3411, 3526, 3548	171.0, 536.6, 642.9
TS12	1024i, 102, 140, 181, 378, 401, 456, 574, 695, 751, 850, 933, 1033, 1173, 1217, 1261, 1324, 1407, 1463, 1493, 1509, 1542, 1691, 3034, 3113, 3372, 3399, 3465, 3527, 3552	185.2, 439.4, 566.9
TS13	1607i, 67, 75, 161, 290, 397, 407, 541, 598, 797, 902, 1017, 1112, 1222, 1257, 1278, 1327, 1457, 1467, 1484, 1698, 2979, 3119, 3291, 3407, 3522, 3574	144.1, 532.8, 609.7
TS14	*1937i, 88, 286, 359, 451, 612, 805, 958, 1047, 1137, 1191, 1242, 1281, 1298, 1351, 1513, 1558, 1717, 1719, 3114, 3258, 3506, 3639, 3654*	*52.4, 221.8, 247.2*
TS15	1342i, 23, 83, 141, 251, 367, 397, 507, 550, 700, 771, 952, 1073, 1131, 1161, 1192, 1347, 1393, 1425, 1428, 1454, 1479, 1486, 1515, 1653, 2933, 3049, 3059, 3095, 3200, 3203, 3392, 3528	137.2, 579.2, 637.5
TS16	557i, 78, 115, 156, 263, 385, 473, 584, 669, 711, 886, 1001, 1135, 1161, 1211, 1407, 1450, 1478, 1484, 1514, 1542, 1617, 1816, 2935, 3043, 3097, 3376, 3438, 3465, 3516	134.4, 554.7, 612.8
TS17	1208i, 58, 78, 148, 246, 359, 479, 640, 729, 791, 967, 1136, 1158, 1203, 1379, 1387, 1456, 1482, 1496, 1516, 1627, 2949, 3048, 3103, 3292, 3447, 3532	110.8, 573.5, 612.8
TS18	*2420i, 149, 252, 415, 444, 683, 779, 978, 1123, 1175, 1207, 1296, 1380, 1496, 1511, 1546, 1559, 1578, 1659, 3075, 3187, 3240, 3487, 3635*	*59.5, 212.7, 227.8*
TS19	481i, 168, 335, 484, 840, 885, 933, 1000, 1145, 1328, 1371, 1533, 1563, 3069, 3170, 3387, 3484, 3529	42.0, 228.5, 252.2
TS20	1983i, 316, 409, 497, 753, 863, 957, 1076, 1187, 1231, 1358, 1421, 1661, 2351, 3094, 3235, 3409, 3560	38.8, 173.9, 200.8
TS21	248i, 58, 192, 332, 404, 448, 700, 1280, 1338, 1407, 1412, 1516, 1574, 3102, 3251, 3273, 3278, 3289	44.8, 308.0, 330.8
TS22	2062i, 178, 452, 557, 862, 1009, 1089, 1106, 1190, 1355, 1429, 1475, 1487, 2486, 2972, 3026, 3106, 3295	41.4, 177.6, 202.1
TS23	871i, 258, 312, 431, 825, 883, 1012, 1041, 1098, 1121, 1150, 1250, 1264, 1437, 1460, 1479, 1511, 1525, 2688, 2863, 2970, 3033, 3099, 3320	51.9, 202.7, 227.9
TS24	1088i, 278, 485, 619, 723, 783, 967, 1025, 1158, 1178, 1319, 1443, 1573, 1645, 3056, 3217, 3396, 3548	37.2, 169.4, 193.5
TS25	2002i, 756, 883, 997, 1076, 1235, 1338, 1464, 2329, 3086, 3208, 3427	13.5, 68.2, 73.6
TS26	2012i, 814, 866, 1085, 1112, 1365, 2346, 3036, 3143	10.5, 62.2, 64.2
TS27	431i, 297, 431, 937, 978, 1373, 1636, 2967, 3027	19.6, 59.1, 66.0
TS28	2253i, 724, 752, 1019, 1133, 1162, 1252, 1368, 1391, 1460, 1586, 2217, 3019, 3131, 3443	21.0, 74.2, 77.2

[a] The unscaled B3LYP/6-31G(d,p) and MP2(full)/6-31G(d,p) theoretical frequencies. Frequencies and moments of inertia optimized at the MP2(full)/6-31G(d,p) level are shown in italics.

TABLE 2: Isodesmic Reaction Analysis[a]

isodesmic reaction	$\Delta H°_{rxn}$	$\Delta_f H°$(298.15 K)	calculation level
$CH_3NHNH_2 + NH_3 = CH_3NH_2 + NH_2NH_2$	6.91	21.36	CBS-Q
$CH_3NHNH_2 + NH_3 = CH_3NH_2 + NH_2NH_2$	6.68	21.59	CBS-QB3
$CH_3NHNH_2 + NH_3 = CH_3NH_2 + NH_2NH_2$	6.67	21.60	G3MP2
$CH_3NHNH_2 + NH_3 = CH_3NH_2 + NH_2NH_2$	6.67	21.60	G3
$CH_3NHNH_2 + NH_3 = CH_3NH_2 + NH_2NH_2$	6.67	21.67	G3B3
$CH_3NHNH_2 + NH_3 = CH_3NH_2 + NH_2NH_2$	6.29	22.40	MPWB1K
$CH_3NHNH_2 + NH_3 = CH_3NH_2 + NH_2NH_2$	7.33	21.36	CCSD(T)//MPWB1K
average $\Delta H_f°_{298}$ value and uncertainty[b]		21.6 ± 0.5	
$C^•H_2NHNH_2 + CH_4 = CH_3NHNH_2 + CH_3$	11.97	62.34	CBS-QB3
$C^•H_2NHNH_2 + NH_3 = CH_3NHNH_2 + NH_2$	14.21	63.87	CBS-QB3
$C^•H_2NHNH_2 + C_2H_6 = CH_3NHNH_2 + C_2H_5$	8.28	62.36	CBS-QB3
average $\Delta H_f°_{298}$ value and uncertainty[b]		62.8 ± 1.8	
$CH_3N^•NH_2 + CH_4 = CH_3NHNH_2 + CH_3$	26.28	48.03	CBS-QB3
$CH_3N^•NH_2 + NH_3 = CH_3NHNH_2 + NH_2$	28.52	49.56	CBS-QB3
$CH_3N^•NH_2 + C_2H_6 = CH_3NHNH_2 + C_2H_5$	22.59	48.05	CBS-QB3
average $\Delta H_f°_{298}$ value and uncertainty[b]		48.5 ± 1.8	
$CH_3NHN^•H + CH_4 = CH_3NHNH_2 + CH_3$	23.77	50.54	CBS-QB3
$CH_3NHN^•H + NH_3 = CH_3NHNH_2 + NH_2$	26.01	52.07	CBS-QB3
$CH_3NHN^•H + C_2H_6 = CH_3NHNH_2 + C_2H_5$	20.08	50.56	CBS-QB3
average $\Delta H_f°_{298}$ value and uncertainty[b]		51.1 ± 1.8	

[a] Units of kcal mol^{-1}. [b] The uncertainties include contributions from uncertainty in ab initio calculations as well as uncertainty in experimental values for the reference compounds. $\Delta_f H°_{298}$ values of reference species, units in kcal mol^{-1}: CH_4, -17.89 ± 0.07, Cox et al.;[28] CH_3, 34.82 ± 0.2, Stull et al.;[29] NH_3, -10.98 ± 0.084, Cox et al.;[30] NH_2, 45.50, Chase;[31] C_2H_6, -20.24 ± 0.12, Cox et al.;[28] C_2H_5, 28.8 ± 0.50, Marshall et al.;[32] CH_3NH_2, -5.5, Stull et al.;[33] NH_2NH_2, 22.79, Chase.[31]

Bohn et al.[25] calculated the N−N bond dissociation enthalpies and enthalpies of formation of hydrazine and its methyl derivatives by DFT and G2MP2 calculations. They determined the $\Delta_f H°$(298.15 K) of MMH to be 19.3 and 22.9 kcal mol^{-1} by nonisodesmic reaction analysis at B3LYP/6-311+G(3df,-2pd)//B3LYP/6-31G(d) and G2MP2 levels, and a value of 22.5 kcal mol^{-1} was recommended, which is consistent with the experimental values of 22.5 and 22.6 kcal mol^{-1}.[26,27] In this work, the $\Delta_f H°$(298.15 K) of MMH calculated by isodesmic reaction analysis at the B3LYP/6-311G(d,p) level is 22.4 kcal mol^{-1}, while the CBS-QB3, G3, G3MP2, G3B3 calculations give almost the same $\Delta_f H°$(298.15 K) value of 21.6 kcal mol^{-1}. In addition, the MPWB1K/6-31+G(d,p) calculation predicts 22.4 kcal mol^{-1}, while the higher level CCSD(T)/6-311++G-(3df,2p)//MPWB1K/6-31+G(d,p) calculation yields a value of 21.4 kcal mol^{-1}. Since the computed $\Delta_f H°$(298.15 K) values agree well at all different calculation levels, the average value of 21.6 ± 0.5 kcal mol^{-1} is recommended for the $\Delta_f H°$(298.15 K) of MMH and was used in the kinetic analysis. From the above data analysis, it is seen that the energy calculation at the CBS-QB3 level combined with isodesmic analysis can predict reliable enthalpy values of hydrazine compounds.

There are three radicals derived from the H loss from the parent MMH: $CH_3N^•NH_2$, $CH_3NHNH^•$, and $CH_2^•NHNH_2$. Three different isodesmic reactions in Table 2 were used to determine the $\Delta_f H°$(298.15 K) of the three radicals based on the calculated $\Delta_f H°$(298.15 K) of the parent MMH. The average values of $\Delta_f H°$(298.15 K) from the isodesmic reactions at the CBS-QB3 level are 48.6, 51.1, and 62.3 kcal mol^{-1} for $CH_3N^•$-NH_2, $CH_3NHNH^•$, and $CH_2^•NHNH_2$ radicals, respectively, with the standard deviation of 0.88 kcal mol^{-1} between the isodesmic reactions. Recently, McQuaid et al.[34] studied the H-atom abstraction from MMH by NO_2 using ab initio and DFT calculations. They reported $CH_2^•NHNH_2$ and $CH_3NHNH^•$ to be 14.2 and 2.0 kcal mol^{-1} higher in energy than $CH_3N^•NH_2$ at the CCSD(T)/6-311++G(3df,2p)//MPWB1K/6-31+G(d,p) level, while our calculated $\Delta_f H°$(298.15 K) of $CH_2^•NHNH_2$ is 14.3 and 2.5 kcal mol^{-1} higher than that of $CH_3N^•NH_2$ on the basis of isodesmic analysis and CBS-QB3 calculation, respectively.

TABLE 3: Bond Dissociation Energies in MMH[a]

CH_3NH-NH_2	63.9
CH_3-NHNH_2	65.7
$CH_3N(-H)NH_2$	79.0
$CH_3NHNH-H$	81.6
NH_2NHCH_2-H	93.4

[a] Units in kcal mol^{-1}.

The data consistency once again demonstrates that the CBS-QB3 method combined with isodesmic analysis yields reliable enthalpy values for methylhydrazine species used in this study.

With the $\Delta_f H°$(298.15 K) of the parent MMH molecule and its radicals derived from the H loss, the $CH_3N(-H)NH_2$, CH_3-$NHNH-H$, and NH_2NHCH_2-H bond dissociation energies (BDEs) at 298 K were determined to be 79.0, 81.6, and 93.4 kcal mol^{-1}, respectively. These values along with the BDEs of CH_3NH-NH_2 and CH_3-NHNH_2 bonds are listed in Table 3. Here we note that recently Song et al.[35] studied the effects of geminal disubstitution on C−H and N−H bond dissociation energies by using ab initio G3, CBS-Q and G3B3 methods, and reported the BDE of $CH_3N(-H)NH_2$ to be 76.5 kcal mol^{-1} at the G3B3 level, which is the best precision for the C−H and N−H BDEs they have found. The difference of 2.5 kcal mol^{-1} on the $CH_3N(-H)NH_2$ bond energy in the two studies is due to the different calculation methods. That is, their value was based on the enthalpy change of the H-atom scission in the gas phase at 298 K from the difference of the total electronic energies of the reactants and products, while our data of this enthalpy change was obtained by the $\Delta_f H°$(298.15 K) from isodesmic analysis and experimental data, which is more accurate. Furthermore, the $CH_3N(-H)NH_2$ bond is 2.5 kcal mol^{-1} weaker than that of $CH_3NHNH-H$ based on our BDE values determined. This is due to the unpaired electron in $CH_3N^•NH_2$ being delocalized by both the CH_3 and NH_2 stabilizing groups, while the unpaired electron in $CH_3NHN^•H$ is delocalized only by the CH_3NH group. The smaller BDE of the $CH_3N(-H)NH_2$ bond than that of the $CH_3NHNH-H$ bond suggests that the formation of the $CH_3N^•$-NH_2 radical is easier from most abstraction reactions. In addition, our calculated C−H bond strength (93.3 kcal mol^{-1})

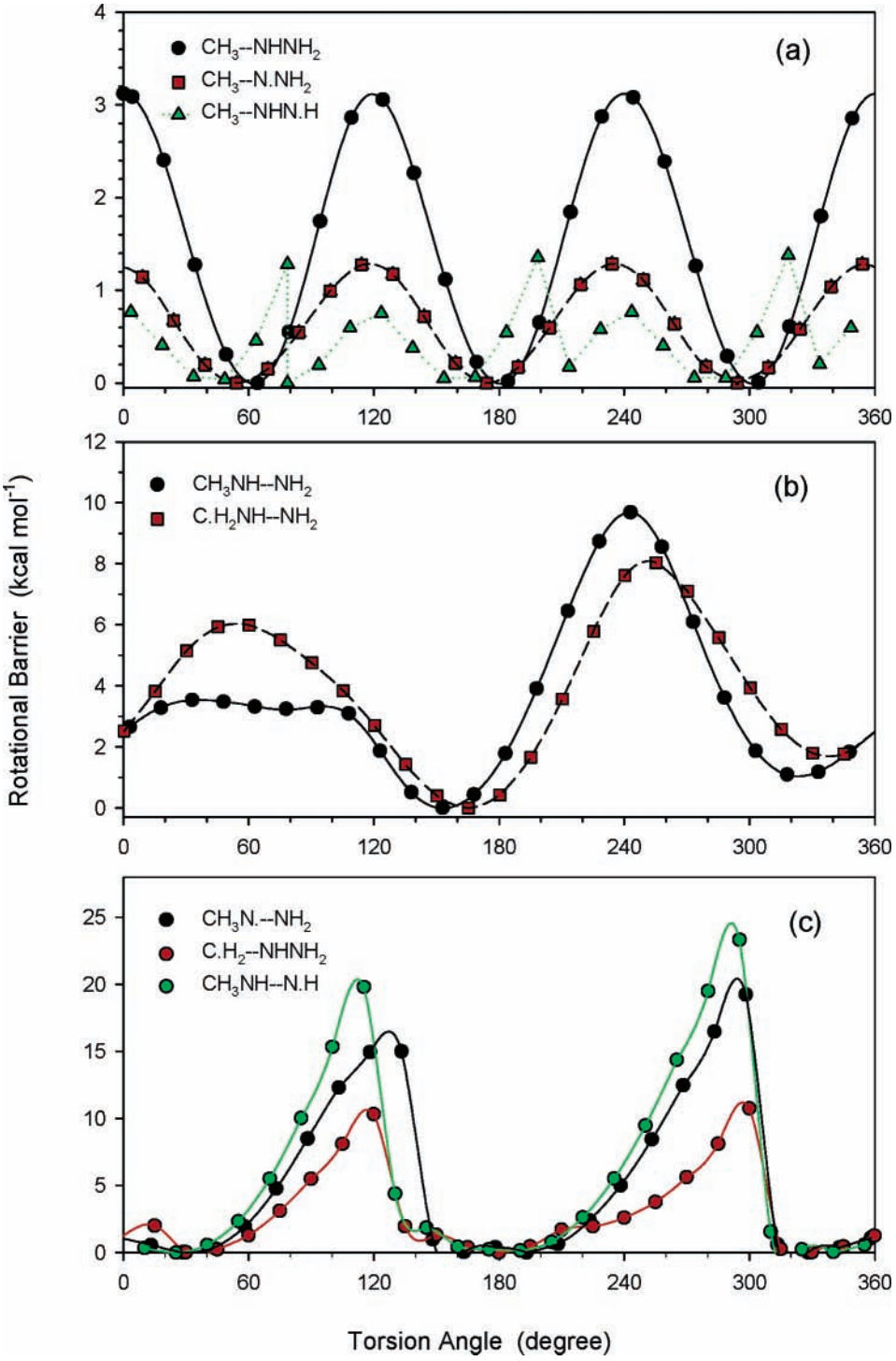

Figure 1. Calculated internal rotational potentials of C−N and N−N bonds for parent CH_3NHNH_2 and its corresponding radicals $CH_3N^{\bullet}NH_2$, $CH_3NHN^{\bullet}H$, and $CH_2^{\bullet}NHNH_2$.

in MMH is similar to that of $H-CH_2NH_2$ (93.9 kcal mol^{-1}),[35] but is weaker than that of $H-CH_2OH$ (96.2 kcal mol^{-1}). The weaker C−H bond strength is due to the stronger stabilization of a lone pair of electrons on the nitrogen and the carbon center through a three-electron interaction. Moreover, it is the reinforced σ-accepting ability and lone-pair-donation effects that account for the greater stabilization of the radicals[36] and result in the weaker bond strength of MMH than that of alcohol and favoring abstraction reactions.

B. Internal Rotation Analysis. The internal rotation potentials of the C−N and N−N bonds of the parent MMH and its corresponding radicals were calculated at the B3LYP/6-311G-(d,p) level, as shown in Figure 1. These potentials were assembled as a, b, and c groups according to their potential curvatures and energy barriers. Figure 1a shows the rotational barriers of the CH_3-N bond for CH_3NHNH_2, $CH_3N^{\bullet}NH_2$, and $CH_3NHN^{\bullet}H$. The methyl rotor of CH_3NHNH_2 has a barrier of 3.1 kcal mol^{-1}, while those of $CH_3-N^{\bullet}NH_2$ and $CH_3-NHN^{\bullet}H$ radicals are only 1.3 kcal mol^{-1}, hence behaving like free rotors. Furthermore, the rotation potential of the $CH_3-NHN^{\bullet}H$ bond exhibits a sixfold barrier behavior, with at least two low-energy conformers, as observed by McQuaid et al.[34]

Figure 1b plots the rotation potentials of the $N-NH_2$ bond for CH_3NHNH_2 and $C^{\bullet}H_2NHNH_2$, showing that they have two

TABLE 4: Thermodynamic Properties for Parent MMH and Its Corresponding Radicals[a]

species		$\Delta_f H°$(298 K)[b]	$S°$(298.15 K)[c]	$C_p°$(300 K)[c]	$C_p°$(400 K)[c]	$C_p°$(500 K)[c]	$C_p°$(600 K)[c]	$C_p°$(800 K)[c]	$C_p°$(1000 K)[c]	$C_p°$(1500 K)[c]
CH_3NHNH_2 (3)[f]	TVR[d]		58.94	12.14	15.58	18.96	21.97	26.85	30.57	36.62
	C−N[e]		4.32	2.11	2.13	2.02	1.88	1.63	1.46	1.23
	N−N[e]		2.50	2.99	3.00	2.81	2.58	2.19	1.94	1.58
CH_3NHNH_2		*21.65*	*65.76*	*17.24*	*20.71*	*23.79*	*26.43*	*30.67*	*33.97*	*39.43*
$CH_3N^{\bullet}NH_2$ (3)[f]	TVR[d]		59.74	11.81	14.76	17.61	20.12	24.20	27.30	32.31
	C−N[e]		5.23	1.67	1.46	1.32	1.23	1.14	1.09	1.04
	N−N[e]		2.44	2.63	2.38	2.15	1.99	1.83	1.77	1.74
$CH_3N^{\bullet}NH_2$		*48.55*	*67.41*	*16.11*	*18.60*	*21.08*	*23.34*	*27.17*	*30.16*	*35.09*
$C^{\bullet}H_2NHNH_2$ (2)[f]	TVR[d]		61.02	12.67	15.70	18.44	20.79	24.51	27.37	32.15
	C−N[e]		3.12	2.29	2.26	2.16	2.06	1.90	1.78	1.59
	N−N[e]		2.04	2.73	2.96	2.98	2.91	2.65	2.36	1.82
$C^{\bullet}H_2NHNH_2$		*62.85*	*66.18*	*17.69*	*20.92*	*23.58*	*25.76*	*29.06*	*31.51*	*35.56*
$CH_3NHN^{\bullet}H$ (3)[f]	TVR[d]		60.03	11.78	14.61	17.43	19.94	24.04	27.17	32.22
	C−N[e]		5.23	1.67	1.46	1.32	1.23	1.14	1.09	1.04
	N−N[e]		2.65	1.46	1.49	1.50	1.51	1.52	1.54	1.58
$CH_3NHN^{\bullet}H$		*51.06*	*67.91*	*14.91*	*17.56*	*20.25*	*22.68*	*26.70*	*29.80*	*34.84*

[a] Thermodynamic properties are referred to a standard state of an ideal gas of at 1 atm. [b] Units of kcal mol^{-1}. [c] Units of cal mol^{-1} K^{-1}. [d] The sum of contributions from translations, vibrations, external rotations, and electronic motions. [e] Contribution from internal rotations. [f] Symmetry number.

equilibrium conformers. The global minima as determined from the C−N and N−N bond rotation potentials support the fact that the inner conformation of MMH (methyl group between the two hydrogen atoms of the NH_2 group) is more stable than the outer form, as indicated by several conformational studies of methylhydrazine.[37−40] The energy of the inner conformation of MMH was determined to be 1.0 kcal mol^{-1} lower than that of the outer conformer at the B3LYP/6-311G(d,p) level. The two barriers that separate the two MMH conformers are 3.5 and 9.7 kcal mol^{-1}, respectively. For the $C^{\bullet}H_2NHNH_2$ radical, the higher energy conformer is 1.7 kcal mol^{-1} higher than the global minima, and the two barriers separating them are 6.0 and 8.0 kcal mol^{-1}, respectively. The relatively higher barrier heights on the N−NH_2 bond are ascribed to the interaction between a lone pair on an N atom and an H atom on the adjacent N atom, since the interatomic distance between them is within 2.0 Å.

Figure 1c shows the twofold rotation potentials of $C^{\bullet}H_2$−$NHNH_2$, $CH_3N^{\bullet}$−NH_2, and CH_3NH−$N^{\bullet}H$ bonds. The higher of the two barriers are 10.7, 19.2, and 23.3, and the lower are 10.3, 15.0, 19.8 kcal mol^{-1}, respectively. The high barriers are due to the strong resonance (the overlap of p orbitals) between these rotational bonds that make them hard to rotate. The resonance can be seen from the planar structures of the radical sites, and also from the shorter bond length of CH_3−$N^{\bullet}NH_2$, $C^{\bullet}H_2$−$NHNH_2$, and CH_3−$NHN^{\bullet}H$ radicals: 1.352, 1.387, and 1.347 Å, respectively, while the N−N and C−N bond lengths of the parent MMH are 1.427 and 1.457 Å, respectively.

Compared with the energies characterized at the CCSD(T)/6-311++G(3df,2p)//MPWB1K/6-31+G(d,p) level,[34] the barrier heights on the N−N bond rotation determined at the DFT level are about 0.8−2 kcal mol^{-1} too high. However, barriers for these N−N bond rotation potentials are relatively high (8−21 kcal mol^{-1}), such that the resulting errors can be ignored for calculations of the contribution from internal rotors to the $S°$(298.15 K) and $C_p°(T)$ values. Table 4 illustrates the calculated values from vibration, translation, and external rotation contributions and also each hindered internal rotation contribution to $S°$(298.15 K) and $C_p°(T)$ for CH_3NHNH_2, $CH_3N^{\bullet}NH_2$, $CH_3NHN^{\bullet}H$, and $C^{\bullet}H_2NHNH_2$ radicals on the basis of the above internal rotation potentials. Table 5 lists the calculated thermochemical properties of the reactants, transition states, and products of the MMH reaction system.

3.2 Reaction Kinetics. *A. Unimolecular Dissociation of MMH.* At temperatures above 800 K, MMH undergoes unimolecular dissociation via several reaction pathways to small products, decomposing significantly above 980 K.[8] A potential energy diagram for the dissociation of MMH calculated at the CBS-QB3 level is shown in Figure 2. It is seen that with the N−N and C−N bond scission, MMH dissociates to the products CH_3NH + NH_2 and CH_3 + $NHNH_2$. Assuming that the activation energy for radical combination is zero, the energy barriers at 298 K for these two channels were calculated to be 65.4 and 66.7 kcal mol^{-1} on the basis of the CBS-QB3 calculation. The former agrees with the BDE of N−N bond in MMH of 65.0 kcal mol^{-1} determined by Bohn et al.[25] from the DFT and G2MP2 calculations. Our further calculations yielded the bond dissociation energies of N−N and C−N fission to be 61.9 and 64.7 kcal mol^{-1} at the CCSD(T)/6-311++G(3df,2p)//MPWB1K/6-31+G(d,p) level, and to be 64.5 and 65.7 kcal mol^{-1} at the MPWB1K/6-31+G(d,p) level. The former is 2 to 3.5 kcal mol^{-1} lower than the CBS-QB3 values, and the latter is 1 to 2 kcal mol^{-1} lower than the CBS-QB3 values. The average values of N−N and C−N BDE values from these calculations were used in the QRRK analysis for our kinetic model. Subsequent dissociations of the H atom at different sites of MMH have higher barriers compared with those of the N−N and C−N bond scissions. Based on the $\Delta H_f°_{298}$ values of the reactant and products, the dissociation barriers were calculated to be 79.0 kcal mol^{-1} to products $CH_3N^{\bullet}NH_2$ + H, 81.6 kcal mol^{-1} to products $CH_3NHNH^{\bullet}$ + H, and 93.4 kcal mol^{-1} to products $C^{\bullet}H_2NHNH_2$ + H, respectively.

Besides bond scissions, MMH can dissociate via three-center or four-center transition states to different products. As shown in Figure 2, by intramolecular transfer of the H atom from the secondary amine group to either the terminal amino group (TS1) or methyl group (TS2), MMH decomposes to two diradical product sets, CH_3N: + HH_3 and CH_4 + $:NNH_2$, with the barriers of 63.1 and 68.2 kcal mol^{-1}, respectively. Furthermore, we found the cleaving N−H bond length to be very different in the three-center transition states of TS1 and TS2. The cleaving N−H bond length is 1.404 Å in TS1 and 1.116 Å in TS2, with the forming N−H and C−H bond lengths of 1.097 and 1.486 Å in the corresponding transition states. The different cleaving N−H bond lengths can be ascribed to the different electronegativities of N and C atoms, since TS1 has a transition center with the N−H−N atoms while TS2 has a transition center with the N−H−C atoms.

The intramolecular transfer of the H atom from the methyl group to the amino group in MMH produces CH_2═NH + NH_3.

TABLE 5: Ideal Gas Phase Thermodynamic Properties[a]

species	$\Delta_f H°$(298 K)[b]	$S°$(298.15 K)[c]	$C_p°$(300 K)[c]	$C_p°$(400K)[c]	$C_p°$(500K)[c]	$C_p°$(600K)[c]	$C_p°$(800K)[c]	$C_p°$(1000 K)[c]	$C_p°$(1500 K)[c]
CH_3NHNH_2	21.65	65.76	17.24	20.71	23.79	26.43	30.67	33.97	39.43
$CH_3N^{\bullet}NH_2$	48.55	67.41	16.11	18.60	21.08	23.34	27.17	30.16	35.09
$C^{\bullet}H_2NHNH_2$	62.85	66.18	17.69	20.92	23.58	25.76	29.06	31.51	35.56
$CH_3NHN^{\bullet}H$	51.06	67.91	14.91	17.56	20.25	22.68	26.70	29.80	34.84
$CH_2{=}NNH_2$	45.46	62.49	14.72	17.23	19.49	21.45	24.66	27.13	31.22
$CH_3N{=}NH_2$	40.10	62.69	12.66	15.10	17.57	19.81	23.48	26.25	30.61
TS1	84.70	63.26	16.65	20.08	23.23	25.98	30.45	33.89	39.45
TS2	89.80	69.23	17.93	21.30	24.26	26.82	30.97	34.20	39.55
TS3	91.10	64.13	15.85	19.67	23.09	26.01	30.60	34.05	39.56
TS4	128.20	64.75	17.18	20.91	24.22	27.03	31.39	34.60	39.58
TS5	130.00	64.55	16.74	20.70	24.14	27.00	31.42	34.66	39.67
TS6	131.60	67.55	17.65	21.26	24.43	27.11	31.35	34.59	39.84
TS7	61.81	83.59	26.89	31.96	36.40	40.18	46.21	50.85	58.39
TS8	68.92	80.68	25.24	29.66	33.53	36.86	42.24	46.43	53.28
TS9	113.47	81.61	24.53	28.67	32.22	35.19	39.85	43.40	49.13
TS10	79.60	68.97	19.62	23.54	27.01	29.97	34.61	38.07	43.55
TS11	66.15	84.24	26.43	31.76	36.43	40.37	46.58	51.32	59.01
TS12	70.93	79.39	24.78	29.74	34.00	37.56	43.09	47.28	54.11
TS13	120.40	82.64	24.72	29.08	32.78	35.83	40.55	44.10	49.88
TS14	86.48	70.77	19.60	23.66	27.31	30.40	35.17	38.69	44.27
TS15	64.03	84.37	25.17	30.42	35.18	39.28	45.83	50.80	58.77
TS16	70.52	80.16	23.67	28.36	32.58	36.23	42.08	46.53	53.74
TS17	116.16	81.90	22.92	27.21	31.06	34.33	39.48	43.35	49.50
TS18	82.03	68.70	18.02	22.03	25.80	29.08	34.23	38.02	43.95
TS19	74.83	66.16	15.36	18.47	21.21	23.49	27.08	29.83	34.43
TS20	100.03	65.29	16.03	18.95	21.53	23.74	27.33	30.09	34.62
TS21	86.67	71.87	17.72	20.05	22.23	24.19	27.49	30.15	34.67
TS22	98.66	67.82	16.12	19.08	21.87	24.29	28.13	30.93	35.15
TS23	79.76	69.47	16.12	20.28	24.30	27.83	33.46	37.61	43.98
TS24	106.89	63.94	15.04	18.61	21.70	24.24	28.09	30.89	35.26
TS25	79.66	56.99	10.33	12.56	14.61	16.37	19.18	21.31	24.75
TS26	119.13	57.09	9.85	11.55	13.07	14.35	16.40	17.95	20.40
TS27	109.99	59.72	12.08	13.56	14.84	15.94	17.68	18.98	21.02
TS28	98.30	56.46	10.91	13.80	16.61	19.07	22.95	25.76	30.00

[a] Thermodynamic properties are referred to a standard state of an ideal gas of pure enantiometer at 1 atm. [b] Units of kcal mol^{-1}. [c] Units of cal mol^{-1} K^{-1}.

The barrier was calculated to be 69.5 kcal mol^{-1} via a four-center transition state TS3. Golden et al.[5] indicated that this path is an actual ammonia-producing mode of the MMH decomposition at the VLPP condition. They estimated that the logarithm of the Arrhenius *A*-factor is 13.1 s^{-1} for this channel, and determined that a critical energy at 298 K of 53.8 kcal mol^{-1} best fitted their experimental data.

The elimination of H_2 from MMH is found by two four-center transition states (TS4, TS5) with two product sets of $CH_3N{=}NH + H_2$ and $CH_2{=}NNH_2 + H_2$. The geometries TS4 and TS5 were found at the MP2/(full)/6-31G(d,p) level, since they failed to be located at the DFT level. The energy barriers at 298 K for the two H_2 elimination channels are high, 106.9 and 108.7 kcal mol^{-1}, by using the MP2 energies. For the H_2 elimination reaction channel via TS4, Golden et al.[5] estimated the logarithm of the *A*-factor to be 13.0 s^{-1}, and a critical energy at 298 K of 56.0 kcal mol^{-1} was found to best fit their experimental k_{uni} at the VLPP conditions. It is noted that, in their study, the rate constant for the H_2 elimination channel was obtained by using the NH_3 and H_2 product peaks for the formation of NH_3 and H_2 and the relations $k_{uni} = k_{NH_3} + k_{H_2}$ and $k_{H_2}/k_{uni} = [H_2]/[NH_3]$. Here the rate constant k_{uni} for the overall MMH decomposition was measured from the disappearance of the parent peak at $m/e = 46$ in the mass spectrum at 923−1273 K, although contributions from $CH_2{=}NH$ and $CH_3N{=}NH$ for deamination and dehydrogenation could not be calibrated. Since the total amount of NH_3 and H_2 formation is greater than that of the MMH decomposed as reported, the accuracy of this rate is limited. Furthermore, since their k_{uni} values reflect the fact that the energy transfer occurred predominantly via gas−wall collisions at very low pressure conditions, they are not the fundamental rates of the MMH thermal decomposition. As subsequently indicated in a review article,[41] the VLPP does not readily provide an independent determination of both the *A*-factor and activation energy parameters, because unimolecular reactions of small molecules are generally not at their high pressure limits for the conditions of milliTorr pressures and temperatures required to observe substantial cleavage of 70−90 kcal mol^{-1} bonds.

The intramolecular interaction of the H atom in the amino group with the methyl group via a four-center transition state TS6 was calculated to have a high barrier of 110.0 kcal mol^{-1}, similar to those channels of dehydrogenation. Obviously, this channel is another mode for methane and hydrazine formation.

The high pressure limit rate constants for these dissociation channels were calculated by canonical transition state theory and fitted by a three-parameter (A, n, E_a) modified Arrhenius equation over the temperature range 300−2000 K by using the THERMKIN program[42] as listed in Table 6. Subsequently, pressure-dependent rate constants were calculated by the QRRK and master equation analysis incorporating these high pressure limit rate parameters. In the QRRK calculations, an energy gradient of 0.5 kcal is used to obtain rate constants as a function of temperature and pressure for dissociation reactions. A $(\Delta E)°_{down}$ of 1000 cal mol^{-1} was approximated in the master equation analysis with nitrogen as the third body. The Lennard-Jones parameters for the collision of MMH with bath gas were derived to be $\sigma = 4.4$ Å and $\epsilon/\kappa = 488.8$ K, by using a group contribution technique that correlates the critical temperature of a substance with its normal boiling point and critical pressure with molecular weight and the correlations of corresponding states.[43] Figure 3 plots the thermally activated MMH dissociation rate constants as a function of 1000/T (K) at 1 atm pressure by

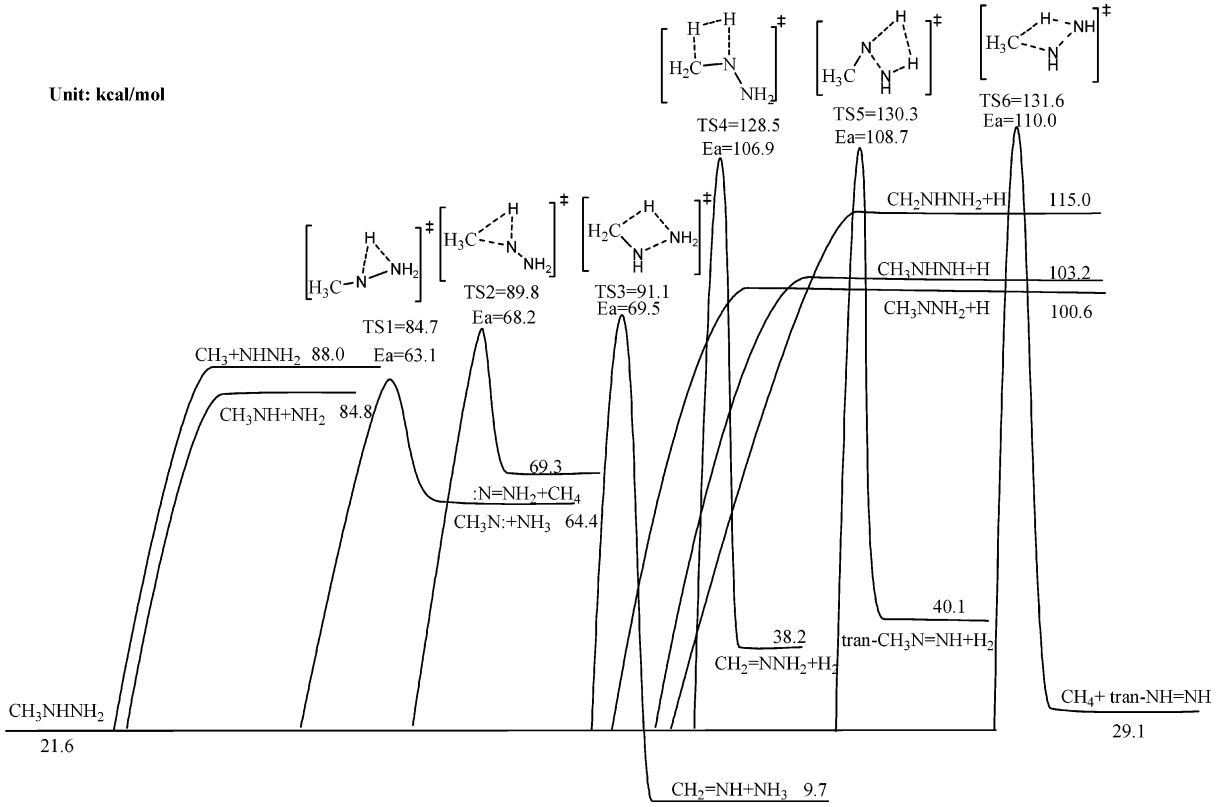

Figure 2. Potential energy diagram of the MMH decomposition system calculated at the CBS-QB3 and CCSD(T)/6-311++G(3df,2p)//MPWB1K/6-31+G(d,p) levels

TABLE 6: Energy Barriers and High Pressure Limit Rate Constants for MMH Decomposition System

no.	reaction	ΔE^a	(A	n	$E_a)^b$
1	$CH_3NHNH_2 \rightarrow TS1 \rightarrow CH_3N + NH_3$	63.1	1.38×10^9	1.360	61.96
2	$CH_3NHNH_2 \rightarrow TS2 \rightarrow NNH_2 + CH_4$	68.2	3.26×10^8	1.809	66.83
3	$CH_3NHNH_2 \rightarrow TS3 \rightarrow CH_2{=}NH + NH_3$	69.5	1.48×10^8	1.503	68.20
4	$CH_3NHNH_2 \rightarrow TS4 \rightarrow CH_2{=}NNH_2 + H_2$	106.9	7.16×10^8	1.374	105.20
5	$CH_3NHNH_2 \rightarrow TS5 \rightarrow CH_3N{=}NH + H_2$	108.7	2.91×10^8	1.477	107.30
6	$CH_3NHNH_2 \rightarrow TS6 \rightarrow NH{=}NH + CH_4$	110.0	3.43×10^9	1.363	108.60
7	$CH_3NHNH_2 + CH_3 \rightarrow TS7 \rightarrow CH_3N^{\bullet}NH_2 + CH_4$	5.4	4.79×10^1	3.385	3.58
8	$CH_3NHNH_2 + NH_2 \rightarrow TS8 \rightarrow CH_3N^{\bullet}NH_2 + NH_3$	1.8	1.65×10^2	3.009	0.87
9	$CH_3NHNH_2 + NH \rightarrow TS9 \rightarrow CH_3N^{\bullet}NH_2 + NH_2$	6.1	1.45×10^2	3.301	4.44
10	$CH_3NHNH_2 + H \rightarrow TS10 \rightarrow CH_3N^{\bullet}NH_2 + H_2$	5.9	2.08×10^7	1.781	4.49
11	$CH_3NHNH_2 + CH_3 \rightarrow TS11 \rightarrow C^{\bullet}H_2NHNH_2 + CH_4$	9.7	2.27×10^1	3.527	7.67
12	$CH_3NHNH_2 + NH_2 \rightarrow TS12 \rightarrow C^{\bullet}H_2NHNH_2 + NH_3$	3.8	1.04	3.603	1.89
13	$CH_3NHNH_2 + NH \rightarrow TS13 \rightarrow C^{\bullet}H_2NHNH_2 + NH_2$	13.1	3.93×10^1	3.567	10.91
14	$CH_3NHNH_2 + H \rightarrow TS14 \rightarrow C^{\bullet}H_2NHNH_2 + H_2$	12.8	7.88×10^7	1.716	11.62
15	$CH_3NHNH_2 + CH_3 \rightarrow TS15 \rightarrow CH_3NHN^{\bullet}H + CH_4$	7.6	3.21×10^2	3.123	5.75
16	$CH_3NHNH_2 + NH_2 \rightarrow TS16 \rightarrow CH_3NHN^{\bullet}H + NH_3$	3.4	5.98×10^1	3.064	2.11
17	$CH_3NHNH_2 + NH \rightarrow TS17 \rightarrow CH_3NHN^{\bullet}H + NH_2$	8.8	6.20×10^2	3.072	7.06
18	$CH_3NHNH_2 + H \rightarrow TS18 \rightarrow CH_3NHN^{\bullet}H + H_2$	8.3	1.68×10^9	1.104	7.29
19	$C^{\bullet}H_2NHNH_2 \rightarrow TS19 \rightarrow CH_2{=}NH + NH_2$	12.0	5.72×10^{12}	0.127	12.24
20	$C^{\bullet}H_2NHNH_2 \rightarrow TS20 \rightarrow CH_2{=}NNH_2 + H$	37.2	9.56×10^{11}	0.303	36.40
21	$CH_3NHN^{\bullet}H \rightarrow TS21 \rightarrow CH_3 + NH{=}NH$	35.6	7.21×10^9	1.507	35.50
22	$CH_3NHN^{\bullet}H \rightarrow TS22 \rightarrow CH_3N{=}NH + H$	45.1	2.43×10^7	1.952	44.60
23	$CH_3N^{\bullet}NH_2 \rightarrow TS20 \rightarrow CH_2{=}NNH_2 + H$	51.5	1.70×10^9	1.176	50.28
24	$CH_3N^{\bullet}NH_2 \rightarrow TS22 \rightarrow CH_3N{=}NH + H$	47.6	1.74×10^8	1.676	47.19
25	$CH_3NHNH_2 + H \rightarrow TS23 \rightarrow CH_3NH + NH_3$	6.1	1.37×10^9	1.120	5.53
26	$CH_2{=}NNH_2 + H \rightarrow TS24 \rightarrow CH_2N + NH_3$	9.3	1.76×10^8	1.309	8.80
27	$CH_3N^{\bullet}H \rightarrow TS25 \rightarrow CH_2{=}NH + H$	36.4	4.81×10^{10}	0.674	35.42
28	$CH_2NH_2 \rightarrow TS25 \rightarrow CH_2{=}NH + H$	43.1	9.32×10^{11}	0.413	42.57
29	$CH_3N \rightarrow TS26 \rightarrow CH_2{=}NH$	43.8	7.97×10^{12}	0.285	43.26
30	$CH_3N \rightarrow TS27 \rightarrow CH_2N + H$	34.6	3.69×10^{11}	0.990	34.78
31	$CH_3NH_2 \rightarrow TS28 \rightarrow CH_2{=}NH + H_2$	103.8	2.31×10^8	1.414	102.24

[a] Energy difference between reactants and transition state. Units of kcal mol^{-1}. [b] Units are $cm^3 \cdot mol \cdot s \cdot cal \cdot K$; $k = AT^n \exp(E_a/RT)$. The rate constants were corrected with tunneling factors.

QRRK calculations. The QRRK analysis indicates that N−N and C−N bond scissions to products $CH_3NH + NH_2$ and $CH_3 + NHNH_2$ are the dominant channels for the unimolecular decomposition of MMH, followed by the dissociation to the products $CH_3N: + HH_3$. Figure 4 plots the rate constants as a function of pressure at 1000 K, and it shows that the dissociation

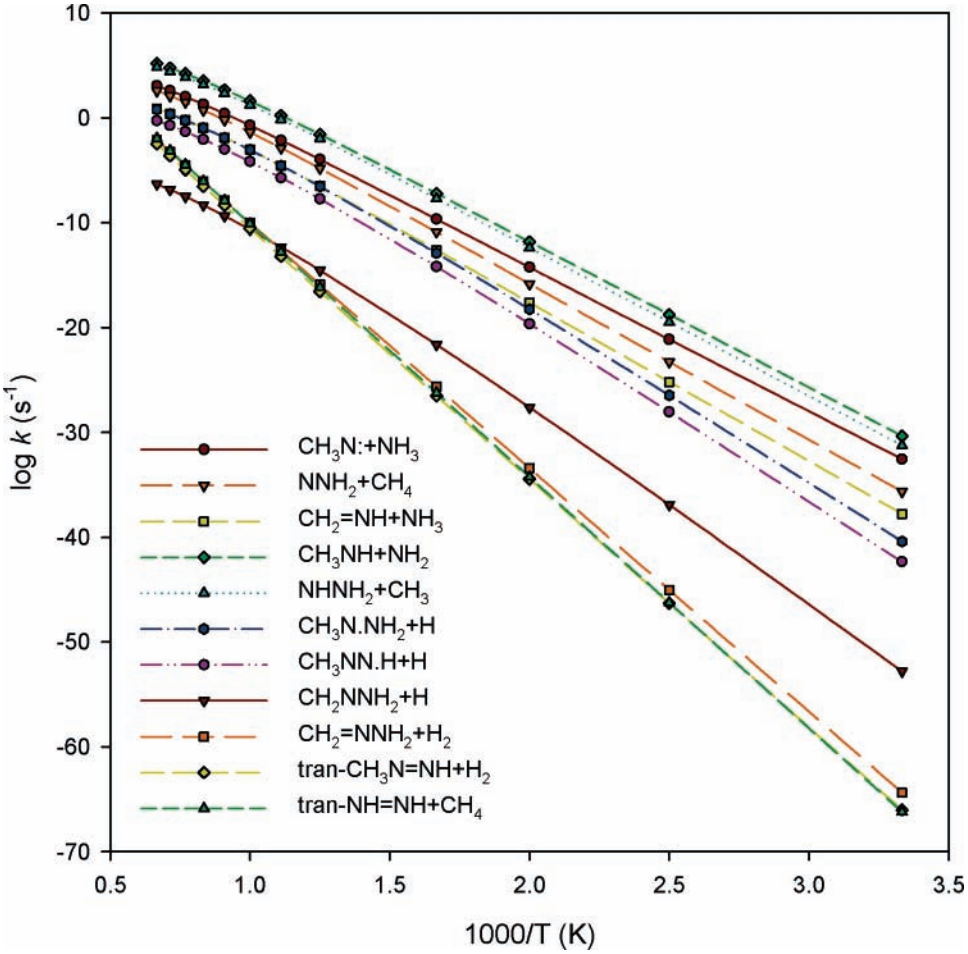

Figure 3. Calculated thermally activated MMH dissociation rate constants at $P = 1$ atm.

rate constants have significant pressure dependence below 10 atm. In particular, the H elimination channels have relatively modest pressure dependence compared to the dominant channels for the N−N and C−N bond scissions. This is because the calculated rate constant $k(E)$ depends on both the energy in excess of the unimolecular threshold and the number of vibrational degrees of freedom.[44] The reactions of the H elimination have less energy in excess of the unimolecular thresholds than those of the N−N and C−N bond scission channels; therefore, they have reduced rates and exhibit profound falloff at low pressures.

B. Abstraction Reactions of MMH. The free radicals produced from the MMH decomposition reactions can abstract H atoms from MMH to form the corresponding $CH_3N^{\bullet}NH_2$, $CH_3NHNH^{\bullet}$, and $C^{\bullet}H_2NHNH_2$ radicals. They are an important class of elementary reactions in the thermal MMH decomposition, although the available experimental or estimated rate constants in the literature are very limited. Hence, the rate constants of abstraction from MMH by H, NH, NH_2, and CH_3 radicals were theoretically calculated in this study.

Specifically, the formation of the $CH_3N^{\bullet}NH_2$ radical by the abstraction of CH_3, NH_2, NH, and H radicals with MMH were found via the transition states TS7, TS8, TS9, and TS10, respectively. Subsequently, the transition states TS11, TS12, TS13, and TS14 were located for the formation of the CH_3-$NHNH^{\bullet}$ radical, and the transition states TS15, TS16, TS17, and TS18 were found for the formation of the $C^{\bullet}H_2NHNH_2$ radical in the above corresponding abstraction reactions. For the abstractions by the H atom, since no geometries were found at the DFT level, the geometries for the transition states TS14, TS18, and TS20 were calculated at the UMP2(full)/6-31G(d,p) level followed by the CCSD(T)/6-31+G(d,p) energy calculation. All other transition state structures for the above abstraction reactions were located by the DFT level of theory followed by CBS-QB3 energy calculations.

Overall, two types of MMH radicals were formed by abstraction reactions: nitrogen-centered and carbon-centered free radicals. By comparing the transition state structures, the corresponding bond lengths for the formation of NH_3, NH_2, H_2, and CH_4 products were found to be different in forming the two types of radicals. Specifically, for the formation of the nitrogen-centered free radicals of $CH_3N^{\bullet}NH_2$ and $CH_3NHNH^{\bullet}$, the cleaving N−H bond is 1.1 Å, and the forming bonds of N−H (NH_3), N−H (NH_2), H−H (H_2), and C−H (CH_4) in their corresponding transition state structures are 1.5, 1.4, 0.99, and 1.5 Å, respectively. For the formation of the carbon-centered free radical of $C^{\bullet}H_2NHNH_2$, the cleaving C−H bond in the transition state structures is 1.2−1.3 Å, and the forming N−H (NH_3), N−H (NH_2), H−H (H_2), and C−H (CH_4) bonds in their corresponding transition state structures are 1.4, 1.3, 0.91, and 1.5 Å, respectively, which are shorter than those in the transition states of nitrogen-centered radicals.

The activation energies at 298 K for the formation of nitrogen-centered radicals were calculated to be 1.8−8.8 kcal mol^{-1}, and those for the formation of carbon-centered radicals are 3.8−12.8 kcal mol^{-1} (see Table 6). The higher energies for the latter are attributed to the stronger C−H bond energies than those of N−H bond as discussed above. As expected, there are not very significant barriers in these abstraction reactions, especially for reactions of MMH with the NH_2 radical, which have activation

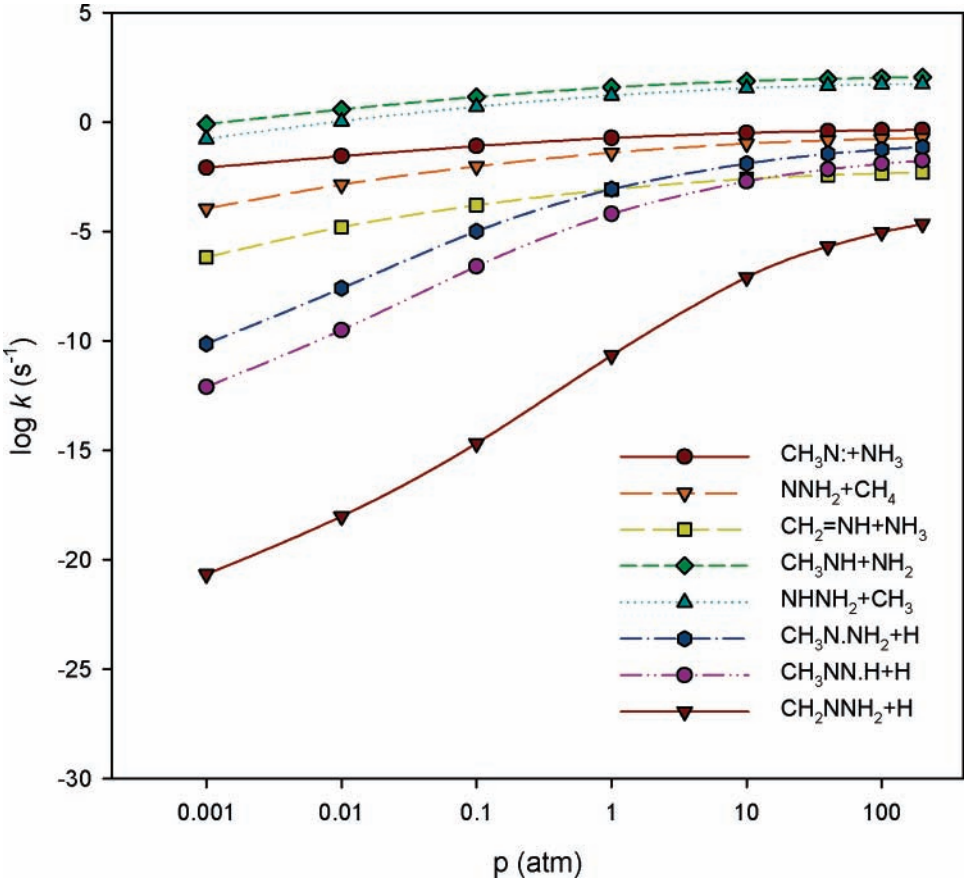

Figure 4. Calculated thermally activated MMH dissociation rate at $T = 1000$ K.

energies at 298 K less than 4 kcal mol^{-1}; hence they are important channels in the MMH thermal dissociation.

C. Dissociation of Radical Products. The $CH_3N^{\bullet}NH_2$, $CH_3NHNH^{\bullet}$, and $C^{\bullet}H_2NHNH_2$ radicals formed from the above abstraction reactions undergo β-scission to dissociate to methanimine, methyldiazene, diazene, and other small radical products. Specifically, the $C^{\bullet}H_2NHNH_2$ radical either dissociates quickly to the products $CH_2{=}NH + NH_2$ with a low barrier of 12.0 kcal mol^{-1} (via TS19), or it can also dissociate to the products $CH_2{=}NNH_2 + H$ with a barrier of 37.2 kcal mol^{-1} (via TS20). Consequently, the $CH_3NHNH^{\bullet}$ radical undergoes β-scission to dissociate to $NH{=}NH + CH_3$ via TS21 (E_a = 35.6 kcal mol^{-1}) and $CH_3N{=}NH + H$ via TS22 (E_a = 45.1 kcal mol^{-1}). For the $CH_3N^{\bullet}NH_2$ radical, it decomposes either to the products $CH_2{=}NNH_2 + H$ with an E_a of 51.5 kcal mol^{-1} or to the products $CH_3N{=}NH + H$ with an E_a of 47.6 kcal mol^{-1}. The transition state structures for these two reaction paths are the same as those of TS20 and TS22, because of the same dissociation products. In summary, all the β-scissions of the MMH radicals have intermediate barriers of 36−52 kcal mol^{-1} except for the N−N bond scission of the $C^{\bullet}H_2NHNH_2$ radical, which has a low-energy barrier of 12.0 kcal mol^{-1}, as shown in Table 6.

The primary radical products $CH_3N^{\bullet}H$, $C^{\bullet}H_2NH_2$, and CH_3N: from the MMH thermal decomposition further undergo isomerization and dissociation reactions to form small products. Similar to the MMH radicals, the $CH_3N^{\bullet}H$ and $C^{\bullet}H_2NH_2$ radicals can dissociate to the same products $CH_2{=}NH + H$ via the same transition state TS25, except with different activation energies, 36.4 and 43.1 kcal mol^{-1}, respectively. The diradical CH_3N: can isomerize to $CH_2{=}NH$ via TS26 (E_a = 43.8 kcal mol^{-1}) and can also decompose to methylene amidogen plus the H atom, $CH_2{=}N + H$, via TS27 with an E_a of 34.6 kcal mol^{-1}. In addition, CH_3NH_2, a secondary product from the MMH decomposition, can dissociate to the products $CH_2{=}NH + H_2$ with a high barrier of 103.8 kcal mol^{-1} via TS28.

D. Electrophilic Substitution Reactions. Besides the H abstraction reactions, the H atom can react with MMH and its derivatives via electrophilic substitution reactions. The rate constants of two electrophilic substitution reactions of $CH_3NHNH_2 + H \rightarrow CH_3NH + NH_3$ and $CH_2{=}NNH_2 + H \rightarrow CH_2N + NH_3$ were calculated in the present study. These two reactions were treated to follow the S_E2 reaction mechanism with single transition states in which the old bond and the newly formed bond are both present, and the corresponding transition state structures were identified by the imaginary frequency in the normal mode coordinate analysis and evaluation of vibrational motion. For the substitution reaction of CH_3NHNH_2 with the H atom, the transition state TS23 was found with the cleaving N−N bond length of 1.446 Å and the forming N−H bond length of 1.150 Å. The activation energy for this reaction was calculated to be 6.1 kcal mol^{-1} at the CBS-QB3 level. For the reaction $CH_2{=}NNH_2 + H \rightarrow CH_2N + NH_3$, the transition state TS24 was located by the forming N−H bond length of 1.378 Å and the cleaving N−N bond length of 1.380 Å with an E_a of 9.3 kcal mol^{-1}.

For the above dissociation, abstraction, and substitution reactions involving MMH decomposition, the Arrhenius parameters for high pressure limit rates were fitted over the temperature range of 300−2000 K, with tunneling effects taken into account. The tunneling factors (Γ) were first determined by Wigner's perturbation equation[24] using the imaginary asymmetric stretching frequency (ν) of the transition state and the activation energy without zero point energy correction (E_c), and then multiplied by high pressure limit rates (k_∞) calculated from canonical transition state theory; finally, the products of k_∞ and

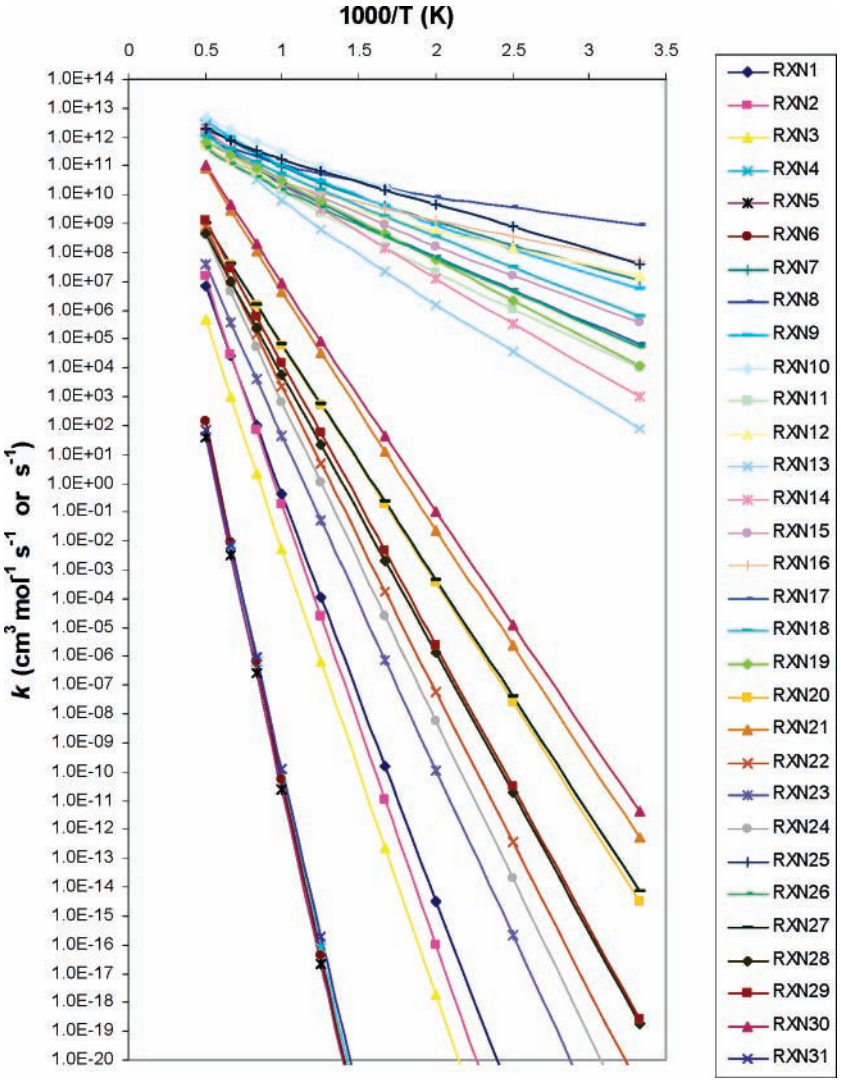

Figure 5. Calculated high pressure limit rate constants of dissociation, abstraction, and substitution reactions in the MMH reaction system.

Γ were fitted by the three Arrhenius parameters, A, n and E_a, for the high pressure limit rates used in kinetic modeling, as listed in Table 6. The tunneling factors as a function of temperature are plotted in Figure S1 of the Supporting Information. It is seen that the tunneling effect for these reaction rates is prominent mainly at low to moderate temperatures, and tends to diminish at higher temperatures as indicated in a previous study.[45] The calculated rate constants in Table 6 are also plotted as a function of temperature in Figure 5. This shows that these rates fall into three groups in magnitude: those of abstraction and substitution are the highest, those of H_2 and CH_4 elimination from MMH and CH_3NH are the lowest due to the high-energy barriers, and between them are those of other MMH dissociation channels and dissociation of the radical products.

3.3. Reaction Mechanism and Modeling Results. An elementary reaction mechanism (750−1500 K, 1atm) was developed to model the overall thermal decomposition rate and compared with experimental data. It consists of 43 species and 160 reactions, as listed in the Supporting Information, Table S2. This reaction mechanism includes the following: (1) dissociation reactions of MMH, intermediates, and small radical products with pressure-dependent rate constants calculated by the QRRK and master equation analysis in this work, (2) abstraction reactions with rate constants calculated in this work, (3) the C−H−N reaction kinetics by Dean and Bozzelli,[46] and (4) the hydrazine decomposition mechanism by Konnov et al.[47] The SENKIN code from the CHEMKIN package[48] was used to calculate the first-order rate of MMH decomposition in the temperature range of 750−1000 K. The plots of the first-order MMH decay rate of $(-\ln [MMH]/[MMH]_0)$ vs time (0.5−50 ms) and the $d[MMH]/dt$ vs the MMH concentration in the temperature range of 750−1000 K are given in Figures S3 and S4 in the Supporting Information.

The overall MMH decomposition rate constant predicted by the present reaction mechanism is compared with experimental data in Figure 6. The comprehensive experimental study by Eberstein et al.[4] for the gas-phase thermal decomposition of MMH was performed in an adiabatic flow reactor at 750−1000 K and atmospheric pressure. Their adiabatic flow reactor was made entirely from quartz to minimize decomposition of the hydrazines in the injection portion, and hot nitrogen carrier gas was flowed through the reactor and mixed rapidly with small quantities of gas-phase reactant, which was injected perpendicularly to the main stream at the throat of the nozzle. The stoichiometry based on gas analysis was reported by the equation $CH_3NHNH_2 = 0.892H_2 + 0.51NH_3 + 0.20CH_4 + 0.51HCN$. In Figure 6, the larger solid points represent our modeling results for the overall MMH thermal decomposition rate, and they agree well with the experimental data of Eberstein et al.[4]

The experimental data of Kerr et al.[3] and Golden et al.[5] at different pressure conditions were also plotted in Figure 6 for comparison. It is noted that our reaction mechanism is not

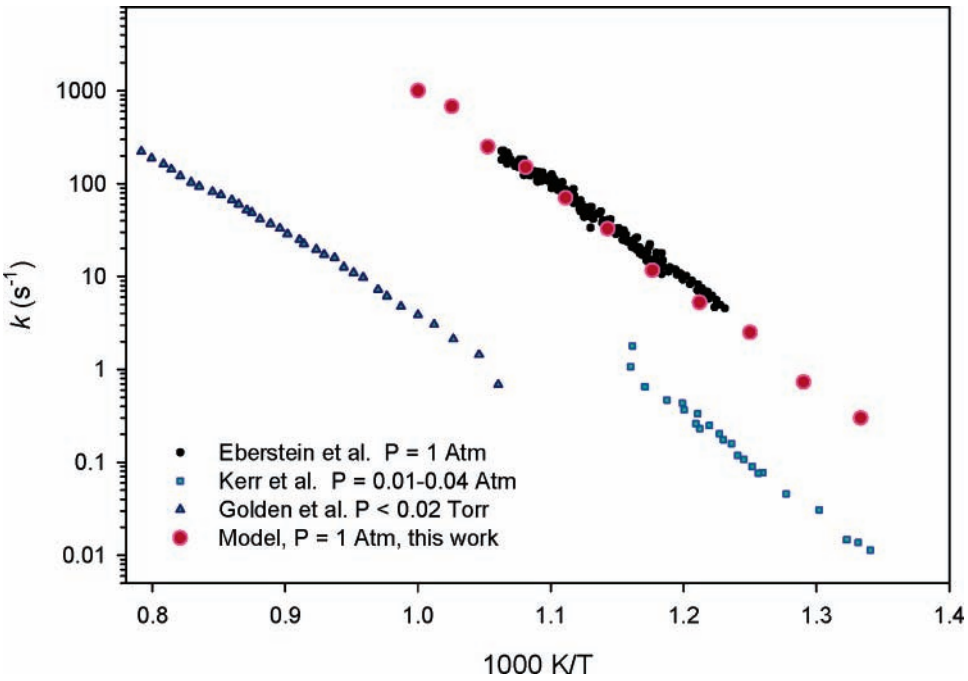

Figure 6. Comparison of predicted rate constant for overall thermal decomposition of MMH with available experimental data.

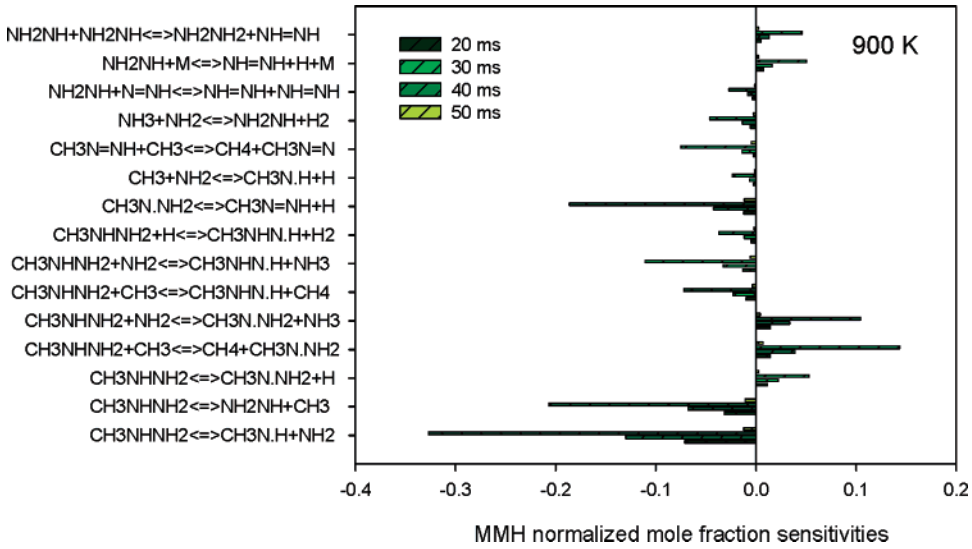

Figure 7. Sensitivity analysis of MMH thermal decomposition at $T = 900$ K and $P = 1$ atm.

feasible to model these experimental data because the experiment by Kerr et al.[3] was performed by the toluene-carrier technique, while the experiment by Golden et al.[5] was conducted at a very low pressure condition at which gas−wall collisions could dominate the energy transfer.

Sensitivity analysis on the reactions of MMH decomposition at the experimental conditions ($T = 900$ K and $P = 1$ atm) is shown in Figure 7. The sensitivity coefficient w_j is defined as $w_j = \partial Y/\partial k_j$ for the disappearance of a species Y, with j as the index of the reaction and k_j as the corresponding reaction coefficient. Figure 7 shows that, before 40 ms, the N−N bond scission of the MMH has the highest sensitivity coefficient for the MMH decomposition, followed by the C−N bond scission of MMH and the dissociation of the $CH_3N^{\bullet}NH_2$ radical to the products $CH_3N{=}NH + H$. Furthermore, the abstraction reactions of $CH_3NHNH_2 + CH_3 \rightarrow CH_3N^{\bullet}NH_2 + CH_4$ and $CH_3NHNH_2 + NH_2 \rightarrow CH_3N^{\bullet}NH_2 + NH_3$ have increased sensitivities to retard the MMH decomposition before 40 ms. Catoire et al.[8] studied ignition delay times for $MMH/O_2/Ar$ gaseous mixtures, and also found the importance of the $CH_3NHNH_2 + NH_2$ reaction, which generates the $CH_3N^{\bullet}NH_2$ radical and reacts with O_2 to produce methyldiazene ($CH_3N{=}NH$) and HO_2. Other sensitive reactions for the MMH decomposition are abstraction of MMH and the major product $CH_3N{=}NH$ with CH_3 and NH_2 radicals. In summary, the reactions for the N−N and C−N bond scission were found to be the major reaction paths for the modeling of MMH homogeneous decomposition at atmospheric conditions, while other reaction channels such as the abstraction of MMH with active radicals and the decomposition of free radical intermediates are also important. We note that the relative importance of these reaction paths is subject to change with time, concentration, pressure, and temperature.

4. Summary

Thermochemical properties of the species in MMH decomposition were calculated using statistical mechanics and molecular parameters from various DFT and ab initio methods. The bond dissociation energies of MMH were determined, and

the different bond strengths of MMH were discussed based on the stability of the forming radicals. The reaction barriers of the thermal decomposition, abstraction, and substitution reactions of MMH were calculated at the CBS-QB3 level, and those of the N−N and C−N bond scissions were determined at the CCSD(T)/6-311++G(3df,2p)//MPWB1K/6-31+G(d,p) level. The high pressure limit rate constants were then calculated by the transition state theory with the correction of tunneling factors. The kinetic parameters of MMH dissociation to intermediate and product channels were calculated by QRRK and master equation analyses as functions of temperature and pressure. An elementary reaction mechanism based on the calculated rate constants, thermochemical properties, and literature data was developed to model the experimental data on overall MMH thermal decomposition rate. The reactions of N−N and C−N bond scission were found to be the major reaction paths for the modeling of MMH homogeneous decomposition at atmospheric conditions.

Acknowledgment. This work was supported by the U.S. Army Research Office.

Supporting Information Available: Optimized structural parameters of 34 stable molecules, radicals and transition states structures are listed in Table S1. A detailed reaction mechanism for MMH thermal decomposition at 1 atm pressure is listed in Table S2. Calculated tunneling factors as a function of temperature for the reaction rates in MMH decomposition system are plotted in Figure S1. The plots of first-order MMH decay and the MMH decomposition rate vs the MMH concentration at the temperature range of 750−1000 K are shown in Figures S2 and S3. This material is available free of charge via the Internet at http://pubs.acs.org.

References and Notes

(1) Catoire, L.; Chaumeix, N.; Paillard, C. *J. Propul. Power* **2004**, *20*, 87.

(2) Schmidt, E. W. *Hydrazine and its derivatives: preparation, properties, applications*, 2nd ed.; Wiley: New York, 2001.

(3) Kerr, J. A.; Sekhar, R. C.; Trotman-Dickenson, A. F. *J. Chem. Soc., B* **1963**, 3217.

(4) Eberstein, I. J.; Glassman, I. *Proc. Combust. Inst.* **1965**, *10*, 365.

(5) Golden, D. M.; Solly, R. K.; Gac, N. A.; Benson, S. W. *Int. J. Chem. Kinet.* **1972**, *4*, 433.

(6) Catoire, L.; Bassin, X.; Dupre, G.; Paillard, C. *Combust. Flame* **1994**, *99*, 573.

(7) Catoire, L.; Bassin, X.; Ingignoli, W.; Dupre, G.; Paillard, C. *Combust. Flame* **1997**, *109*, 37.

(8) Catoire, L.; Ludwig, T.; Bassin, X.; Dupre, G.; Paillard, C. *Proc. Combust. Inst.* **1998**, *27*, 2359.

(9) Catoire, L.; Dupre, G.; Paillard, C.; Elaissi, A. *J. Propul. Power* **2001**, *17*, 1085.

(10) Catoire, L.; Luche, J.; Dupré, G.; Paillard, C. *Shock Waves* **2001**, *11*, 97.

(11) Frisch, M. J.; Trucks, G. W.; Schlegel, H. B.; Scuseria, G. E.; Robb, M. A.; Cheeseman, J. R.; Montgomery, J. A., Jr.; Vreven, T.; Kudin, K. N.; Burant, J. C.; Millam, J. M.; Iyengar, S. S.; Tomasi, J.; Barone, V.; Mennucci, B.; Cossi, M.; Scalmani, G.; Rega, N.; Petersson, G. A.; Nakatsuji, H.; Hada, M.; Ehara, M.; Toyota, K.; Fukuda, R.; Hasegawa, J.; Ishida, M.; Nakajima, T.; Honda, Y.; Kitao, O.; Nakai, H.; Klene, M.; Li, X.; Knox, J. E.; Hratchian, H. P.; Cross, J. B.; Adamo, C.; Jaramillo, J.; Gomperts, R.; Stratmann, R. E.; Yazyev, O.; Austin, A. J.; Cammi, R.; Pomelli, C.; Ochterski, J. W.; Ayala, P. Y.; Morokuma, K.; Voth, G. A.; Salvador, P.; Dannenberg, J. J.; Zakrzewski, V. G.; Dapprich, S.; Daniels, A. D.; Strain, M. C.; Farkas, O.; Malick, D. K.; Rabuck, A. D.; Raghavachari, K.; Foresman, J. B.; Ortiz, J. V.; Cui, Q.; Baboul, A. G.; Clifford, S.; Cioslowski, J.; Stefanov, B. B.; Liu, G.; Liashenko, A.; Piskorz, P.; Komaromi, I.; Martin, R. L.; Fox, D. J.; Keith, T.; Al-Laham, M. A.; Peng, C. Y.; Nanayakkara, A.; Challacombe, M.; Gill, P. M. W.; Johnson, B.; Chen, W.; Wong, M. W.; Gonzalez, C.; Pople, J. A. Gaussian 03, revision C.02; Gaussian, Inc.: Wallingford, CT, 2004.

(12) Lee, C.; Yang, W.; Parr, R. G. *Phys. Rev. B* **1988**, *37*, 785.

(13) Ochterski, J. W.; Petersson, G. A.; Montgomery, J. A., Jr. *J. Chem. Phys.* **1996**, *104*, 2598.

(14) Montgomery, J. A.; Frisch, J. W.; Ochterski, J. W.; Petersson, G. A. *J. Chem. Phys.* **1999**, *110*, 2822.

(15) Curtiss, L. A.; Redfern, P. C.; Raghavachari, K.; Rassolov, V.; Pople, J. A. *Chem. Phys. Lett.* **1999**, *313*, 600.

(16) Baboul, A. G.; Curtiss, L. A.; Redfern, P. C.; Raghavachari, K. *J. Chem. Phys.* **1999**, *110*, 7650.

(17) Curtiss, L. A.; Redfern, P. C.; Raghavachari, K.; Rassolov, V.; Pople, J. A. *J. Chem. Phys.* **1999**, *110*, 4703.

(18) Zhao, Y.; Truhlar, D. G. *J. Phys. Chem. A* **2004**, *108*, 6908.

(19) Purvis, G. D.; Bartlett, R. J. *Chem. Phys. Lett.* **1989**, *157*, 479.

(20) *GaussView*, 3.06 ed.; Gaussian, Inc.: Pittsburgh, PA, 2003.

(21) Scott, A. P.; Radom, L. *J. Phys. Chem.* **1996**, *100*, 16502.

(22) Ritter, E. R.; Bozzelli, J. W. *Int. J. Chem. Kinet.* **1991**, *23*, 767.

(23) Lay, T. H.; Bozzelli, J. W.; Dean, A. M.; Ritter, E. R. *J. Phys. Chem.* **1995**, *99*, 14514.

(24) Shavitt, I. *J. Chem. Phys.* **1959**, *31*, 1359.

(25) Bohn, M. A.; Klapotke, T. M. *Z. Naturforsch., B* **2004**, *59b*, 148.

(26) Majer, V.; Svoboda, V. *Enthalpies of Vaporization of Organic Compounds: A Critical Review and Data Compilation*; Blackwell Scientific: Oxford, 1985.

(27) Pedley, J. B.; Naylor, R. D.; Kirby, S. P. *Thermochemical Data of Organic Compounds*, 2nd ed.; Chapman and Hall: London, New York, 1986.

(28) Cox, J. D.; Pilcher, G. *Thermochemistry of Organic & Organometallic Compounds*; Academic Press: London, New York, 1970.

(29) Stull, D. R.; Prophet, H. *JANAF Thermochemical Tables*, 2nd ed.; U.S. Government Printing Office: Washington, DC, 1970.

(30) Cox, J. D.; Wagman, D. D.; Medvedev, V. A. *CODATA Key Values for Thermodynamics*; Hemisphere: New York, 1984; Vol. 1.

(31) Chase, M. W., Jr. *J. Phys. Chem. Ref. Data, Monogr.* **1998**, No. 9.

(32) Marshall, P. *J. Phys. Chem. A* **1999**, *103*, 4560.

(33) Stull, D. R.; Westrum, E. F.; Sinke, G. C. *The Chemical Thermodynamic of Organic Compounds*; Krieger: Malabar, FL, 1987.

(34) McQuaid, M. J.; Ishikawa, Y. *Phys. Chem. A* **2006**, *110*, 6129.

(35) Song, K.-S.; Liu, L.; Guo, Q.-X. *Tetrahedron* **2004**, *60*, 9909.

(36) Henry, D. J.; Parkinson, C. J.; Mayer, P. M.; Radom, L. *J. Phys. Chem. A* **2001**, *105*, 6750.

(37) Durig, J. R.; Gounev, T. K.; Zheng, C.; Choulakian, A.; Verma, V. N. *J. Phys. Chem. A* **2002**, *106*, 3395.

(38) Murase, N.; Yamanouchi, K.; Egawa, T.; Kuchitzu, K. *J. Mol. Struct.* **1991**, *242*, 409.

(39) Durig, J. R.; Zheng, C. *Vib. Spectrosc.* **2002**, *30*, 59.

(40) Ma, B.; Lii, J.-H.; Chen, K.; Allinger, N. L. *J. Phys. Chem.* **1996**, *100*, 11297

(41) McMillen, D. F.; Golden, D. M. *Annu. Rev. Phys. Chem.* **1982**, *33*, 493.

(42) Sheng, C. Representative Hydrocarbon Oxidation Model and Detailed Mechanism for Combustion of a Complex Solid Fuel in a Pilot Scale Incinerator. Ph.D. Dissertation, New Jersey Institute of Technology, 2002.

(43) Wang, H.; Frenklach, M. *Combust. Flame* **1994**, *96*, 163.

(44) Steinfeld, J. I.; Francisco, J. S.; Hase, W. *Chemical kinetics and dynamics*; Prentice Hall: Upper Saddle River, NJ, 1999.

(45) Zheng, X. L.; Sun, H. Y.; Law, C. K. *J. Phys. Chem. A* **2005**, *109*, 9044.

(46) Dean, A. M.; Bozzelli, J. W. In *Gas-Phase Combustion Chemistry II*; Springer-Verlag: New York, 1999; Chapter 2: Combustion Chemistry of Nitrogen.

(47) Konnov, A. A.; Ruyck, J. D. *Combust. Flame* **2001**, *124*, 106.

(48) Kee, R. J.; Rupley, F. M.; Miller, J. A.; Coltrin, M. E.; Grcar, J. F.; Meeks, E.; Moffat, H. K.; Lutz, A. E.; G. Dixon-Lewis, M.; Smooke, D.; Warnatz, J.; Evans, G. H.; Larson, R. S.; Mitchell, R. E.; Petzold, L. R.; Reynolds, W. C.; Caracotsios, M. W.; Stewart, E.; Glarborg, P.; Wang, C.; McLellan, C. L.; Adigun, O.; Houf, W. G.; Chou, C. P.; Miller, S. F.; Ho, P.; Young, P. D.; Young, D. J. *CHEMKIN* Release 4.0.2, Reaction Design, San Diego, CA, 2005.